

Cascading Dark Energy

KAZEM REZAZADEH,¹ AMJAD ASHOORIOON,¹ AND DANIEL GRIN²

¹*School of Physics, Institute for Research in Fundamental Sciences (IPM), P.O. Box 19395-5531, Tehran, Iran*

²*Department of Physics and Astronomy, Haverford College, 370 Lancaster Avenue, Haverford, PA 19041, United States*

(Received ???; Revised ???; Accepted ???)

Submitted to ApJ

ABSTRACT

The standard cosmological model is in the midst of a stress test, thanks to the tension between supernovae-based measurements of the Hubble constant H_0 and inferences of its values from Cosmic Microwave Background (CMB) anisotropies. Numerous explanations for the present-day cosmic acceleration require the presence of a new fundamental scalar field, as do Early Dark Energy (EDE) solutions to the Hubble tension. This raises the possibility that multiple fields cooperatively contribute to the dark energy component in bursts throughout cosmic time due to distinct initial conditions and couplings. Here, this Cascading Dark Energy (CDE) scenario is illustrated through a realization that effectively reduces to a two-field model, with two epochs in which dark energy is cosmologically significant. The model is compared to measurements of the CMB, baryon acoustic oscillations, as well as both PANTHEON and SH0ES observations of Type-Ia supernovae. Neglecting the linear perturbations, it is found that this scenario ameliorates the Hubble tension, improving over purely late-time models of dark energy, and the agreement between the galaxy survey measurements of baryon acoustic oscillations.

Keywords: cosmology: theory — dark energy — cosmological parameters — H_0 tension

1. INTRODUCTION

Measurements of the present-day Hubble parameter (the Hubble constant H_0) from supernovae (Riess et al. 2016, 2018, 2019, 2022a,b; Murakami et al. 2023) disagree with the value inferred from the Cosmic Microwave Background (CMB) data (Aghanim et al. 2020a,b,c) fit the Λ CDM model. More specifically, CMB power spectra determined by the *Planck* collaboration yield a preferred value of $H_0 = 67.4 \pm 0.6 \text{ km s}^{-1} \text{ Mpc}^{-1}$ (Aghanim et al. 2020a). Similarly, measurements of the acoustic horizon by the Dark Energy Survey (DES), combined with constraints to the baryon density from Big-Bang Nucleosynthesis (BBN) abundances, yield the value $H_0 = 67.4_{-1.2}^{+1.1} \text{ km s}^{-1} \text{ Mpc}^{-1}$ (Abbott et al. 2018a). Strong-lensing time delays also probe H_0 , but realistic error bars (which include the mass-sheet degeneracy) leave these measurements consistent with both CMB and supernovae values.¹

eracy) leave these measurements consistent with both CMB and supernovae values.¹

In contrast, observations of Type-Ia supernovae, tethered to a distance ladder obtained using Hubble Space Telescope (HST) measurements of 70 long-period Cepheids in the Large Magellanic Cloud, imply a substantially different value, $H_0 = 73.3 \pm 1.1 \text{ km s}^{-1} \text{ Mpc}^{-1}$ (Riess et al. 2022b). This is known as the “Hubble tension”. Although this discrepancy might be caused by systematic effects in the data (though none seem sufficient so far), it could alternatively herald exciting new physics beyond the Λ CDM concordance model.

Many proposals have been suggested to resolve this tension [see, e.g. (Umiltà et al. 2015; Karwal & Kamionkowski 2016; Poulin et al. 2018b, 2019; Pandey et al. 2020; Agrawal et al. 2019; Vagnozzi

Corresponding author: Kazem Rezazadeh
kazem.rezazadeh@ipm.ir

¹ Strong-lensing time delays also probe H_0 (Bonvin et al. 2017; Birrer et al. 2019), but realistic error bars (which include the mass-sheet degeneracy) leave these measurements consistent with both CMB and supernovae values (Millon et al. 2020; Shajib et al. 2023).

2020; Smith et al. 2020a; Davari et al. 2020; Sola et al. 2020; Smith et al. 2020b; Krishnan et al. 2021)], some of which (late-time resolutions) invoke modifications to Λ CDM which become predominant near the current cosmological epoch, others of which cause modifications to the cosmic budget at early times (early-time resolutions, which modify cosmic evolution around or before matter-radiation equality).

Among the proposed late-time resolutions are phantom-like Dark Energy (DE) (Di Valentino et al. 2016, 2017a), a vacuum phase transition (Di Valentino et al. 2018), interacting DE (Kumar & Nunes 2016; Di Valentino et al. 2017b), and modified theories of gravity (Barreira et al. 2014; Umiltà et al. 2015; Ballardini et al. 2016; Renk et al. 2017; Belgacem et al. 2018; Nunes 2018; Lin et al. 2019). These scenarios (Di Valentino et al. 2017a,b; Addison et al. 2018) and more model-independent generalizations of them (Bernal et al. 2016; Zhao et al. 2017; Poulin et al. 2018a) are highly constrained by the data, especially by measurements of the Baryon Acoustic Oscillations (BAO) (Beutler et al. 2011; Ross et al. 2015; Alam et al. 2017) in galaxy surveys. Late-time resolutions to the Hubble tension usually suffer from some fundamental shortcomings, such as being a worse fit to CMB data than Λ CDM, fine-tuning issues, inappropriate use of an H_0 prior (Efstathiou 2021), and conflicts with the ages of globular clusters (Jimenez et al. 2019; Valcin et al. 2020, 2021), as discussed in Bernal et al. (2021).

In most realizations of early-time solutions, the sound horizon is reduced by introducing additional radiation energy density to the matter-energy content of the Universe. Such scenarios are also constrained by BAO and the high- ℓ CMB power spectrum (Poulin et al. 2019; Smith et al. 2020a; Karwal et al. 2022; Poulin et al. 2021; Murgia et al. 2021). For example, in Early Dark Energy (EDE) scenarios, the Universe contains a component (typically a scalar field) whose behavior is like a cosmological constant prior to a critical redshift (preceding matter-radiation equality) and dilutes as fast or faster than radiation (Poulin et al. 2019; Smith et al. 2020a) subsequently.

Aside from the Hubble tension, there is another disagreement between cosmological data sets, known as the S_8 tension. This tension reflects the fact that the value of $S_8 \equiv \sigma_8 \sqrt{\Omega_m/0.3}$ (where Ω_m is the today's matter density and σ_8 denotes the variance of matter perturbations within 8Mpc/ h today) implied by the CMB (when fit by the Λ CDM model) does not agree with the value inferred from galaxy weak-lensing measurements of the amplitude of matter density fluctuations in the late-time

Universe (Abbott et al. 2018b; Hildebrandt et al. 2020; Hikage et al. 2019; Asgari et al. 2021; Loureiro et al. 2022; Abbott et al. 2022; Zürcher et al. 2022).

Results from Dark Energy Survey (DES) 3-year data yield the constraint $S_8 = 0.797^{+0.015}_{-0.013}$ (68% CL) (Zürcher et al. 2022), in contrast with the value $S_8 = 0.832 \pm 0.013$ (68% CL) implied by the best-fit value for the amplitude of the scalar density power spectrum from Planck 2018 TT,TE,EE +lowE+CMB lensing data, assuming Λ CDM (Aghanim et al. 2020a). Although EDE models can alleviate the H_0 tension, they tend to exacerbate the S_8 tension (Hill et al. 2020; Ivanov et al. 2020; Murgia et al. 2021) and worsen fits to BAO data [see, e.g. (Poulin et al. 2019; Smith et al. 2020a; Murgia et al. 2021)].

It is interesting to consider the possibility that these tensions (and the required fine-tuning of EDE models) could be alleviated by a richer dark energy sector, for example, if there are multiple epochs of cosmic acceleration driven by one field (Niedermann & Sloth 2021, 2022; Freese & Winkler 2021; Allali et al. 2021), or if many scalar fields acting over time could yield better concordance between cosmological data sets (Sabla & Caldwell 2021; Ramadan et al. 2024).

In this paper, we explore if a resolution for the Hubble tension can be found in the Cascading Dark Energy (CDE) scenario, in which multiple scalar fields contribute to dark energy, analogously to the assisted inflationary scenario (Liddle et al. 1998). CDE is motivated by recent developments in string theory, such as the swampland conjecture (Vafa 2005; Ooguri & Vafa 2007; Obied et al. 2018). CDE reduces the Hubble tension primarily by altering the early-time sound horizon, like the standard EDE scenario.

Some of the fields, however, drop out of sync with the others due to their initial conditions - that is to say that they no longer roll slowly (with nearly constant energy density) even as other fields jointly continue to behave as dark energy. The evolution of each field becomes significant after the Hubble parameters drop below some specific value which depends on the effective mass of the field as well as the background energy density. After that, the field begins to oscillate around the local minimum of its potential and loses its energy accordingly.

In the simplest realization, our model will reduce to two fields, allowing us to treat the dynamics of each field separately without resorting to an effective one-field approximation, as was done in, e.g. Sabla & Caldwell (2021). Multi-field models for dark energy are well motivated by considerations from string theory, such as the axiverse scenario (Arvanitaki et al. 2010), in which a broad mass spectrum of ultra-light axions

could contribute to both dark matter and dark energy (Hlozek et al. 2015; Marsh 2016). They may contribute to explaining the “why now” question for the late-time dark energy driving present-day cosmic acceleration (Kamionkowski et al. 2014; Emami et al. 2016). At earlier times, multiple-field scenarios could help reduce the fine-tuning needed for EDE models to succeed. Here, we consider the possibility that some dark energy fields are relevant near equality/recombination, while others are more relevant today.

We investigate the behavior of the Hubble parameter and the field configuration in our setup. Both fields couple to gravity minimally, and their kinetic terms are assumed to be canonical. The potentials of both fields in the simplest realization are considered to be quartic, although one can assume that they are different, as we will explain later. In our work, we check the consistency of the CDE scenario with the existing data, including the CMB (Aghanim et al. 2020a,b,c), Pantheon SN (Scolnic et al. 2018), BAO (Alam et al. 2017; Ross et al. 2015; Beutler et al. 2012), and Riess et al. (2019) (SH0ES) measurements. We use Monte Carlo Markov Chains (MCMC) simulations to constrain CDE model parameters using cosmological data. We compare the CDE scenario with the concordance Λ CDM model, as well as with a single-field canonical scalar field that couples minimally to gravity and has a quartic potential.

Furthermore, we compare our model to the Rock ‘n’ Roll (RnR) quartic model (Agrawal et al. 2019), which includes a cosmological constant and an oscillating scalar field acting as EDE. It is known that in the case of a full $(1 - \cos\theta)^n$ potential [as considered in Poulin et al. (2019); Smith et al. (2020a)], anharmonic deviations from quadratic behavior are important in driving perturbative mode evolution towards behavior that more optimally addresses the H_0 tension than the Rock ‘n’ Roll scenario. Nevertheless, we compare our CDE scenario to the Rock ‘n’ Roll realization of EDE, as it provides a useful foil for comparing single- and multi-field models with similar potentials.

We compare the result of our two-field CDE scenario for H_0 with the results of the Λ CDM model, the single-field DE model, and also the Rock ‘n’ Roll scenario. We want to know if the H_0 tension can be resolved via the CDE framework, and if so, whether it has any advantages. The full dynamics of *two* coherently oscillating scalar fields coupled through gravity can be complicated and potentially computationally expensive [e.g. Chen & Soda (2023)], especially in the presence of perturbations. A complete analysis with minimal priors would ultimately require a careful analysis of resonance between the two fields (both for perturbations and the

background), as well as multi-field initial conditions for the perturbations. In this work, our primary aim is to assess the relative merits of CDE compared with the Rock ‘n’ Roll model and to see if the addition of only one additional field can significantly impact EDE’s resolution of the Hubble tension. We comment more on these simplifications later in the paper.

We compare the implied value of S_8 for the empirically allowed parameter space of our model with that of these other models. Altogether, we find that the two-field CDE model ($\chi^2_{\text{total}} = 3828.02$) fits the observational data better than the Λ CDM ($\chi^2_{\text{total}} = 3832.03$) and single-field DE ($\chi^2_{\text{total}} = 3832.17$) models. The result of our two-field CDE model is more consistent with the Riess et al. (2019) measurement in comparison with the predictions of the Λ CDM and single-field DE models, and therefore our model can ameliorate the H_0 tension that exists between cosmological data from different sources. Due to the resemblance of our two-field model to the Rock ‘n’ Roll model with $n = 2$, we contrast our setup with that model too. We find that the predictions of quartic two-field CDE are very close to the Rock ‘n’ Roll model with $n = 2$, although the late-time evolution of the dark energy at late times in our model yields a modestly better fit to the BAO data. Overall, however the Rock ‘n’ Roll model still fits the data sets better due to the worse fit of CDE to the SH0ES data.

The rest of this paper is structured as follows: In Sec. 2, we introduce the CDE model and explain its theoretical motivation. Then, in Sec. 3, we explore the two-field realization of the CDE model and present its equations of motion. Subsequently, in Sec. 4, we describe the setup of a Monte Carlo Markov Chain (MCMC) analysis used to test a two-field CDE scenario using cosmological data. We discuss results in Sec. 5. We present our conclusions in Sec. 6, where we also put forward avenues to expand and further test the CDE scenario.

2. SETUP OF CASCADING DARK ENERGY

We consider $N + 1$ scalar fields with quartic monomial potentials, with $N \gg 1$, $V(\phi_i) = \frac{\lambda}{4}\phi_i^4$, $i = 1 \dots N + 1$, with the Lagrangian

$$S = \int \sqrt{-g} d^4x \left[\sum_{i=1}^{N+1} \left(\frac{1}{2} \partial_\mu \phi_i \partial^\mu \phi_i - \frac{\lambda}{4} \phi_i^4 \right) \right]. \quad (1)$$

For simplicity, we have assumed that the quartic couplings of all the fields are the same. In principle, these scalar fields can have different initial conditions. We assume the swampland distance conjecture, under which these fields can at most transverse M_P in the field space before a tower of massless species appears. We thus assume that the initial conditions of all the fields are

sub-Planckian. Following the de-Sitter swampland conjecture, we also assume that the relative slope of the potential should not be very flat, yielding the constraint that

$$M_P \frac{V'}{V} \gtrsim c = \mathcal{O}(1). \quad (2)$$

Let us assume that all the first N fields have the same initial conditions, which are different from that of the $(N + 1)$ -th field,

$$\begin{aligned} \phi_1 = \phi_2 = \dots = \phi_N = \phi_0, \\ \phi_{N+1} = \chi_0. \end{aligned} \quad (3)$$

Then the effective Lagrangian of ϕ_0 and χ_0 can be written as,

$$\begin{aligned} S = \int d^4x \sqrt{-g} \left(\frac{N}{2} \partial_\mu \phi_0 \partial^\mu \phi_0 + \frac{1}{2} \partial_\mu \chi_0 \partial^\mu \chi_0 \right. \\ \left. - N \frac{\lambda}{4} \phi_0^4 - \frac{\lambda}{4} \chi^4 \right). \end{aligned} \quad (4)$$

We introduce the new effective fields, ϕ and χ ,

$$\begin{aligned} \phi &\equiv \sqrt{N} \phi_0, \\ \chi &\equiv \chi_0, \end{aligned} \quad (5)$$

to make the kinetic term of the ϕ_0 field in the Lagrangian canonical, which leads to the Lagrangian

$$S = \int \sqrt{-g} d^4x \left(\frac{1}{2} \partial_\mu \phi \partial^\mu \phi + \frac{1}{2} \partial_\mu \chi \partial^\mu \chi - \frac{\lambda_\phi}{4} \phi^4 - \frac{\lambda_\chi}{4} \chi^4 \right), \quad (6)$$

where

$$\begin{aligned} \lambda_\phi &\equiv \frac{\lambda}{N}, \\ \lambda_\chi &\equiv \lambda, \end{aligned} \quad (7)$$

Although the fields ϕ_i , $i = 1 \dots N + 1$, cannot be super-Planckian due to swampland conjecture (Ooguri & Vafa 2007), the fields ϕ can be super-Planckian due to the large dressing factor \sqrt{N} if $N \gg 1$.

With these initial conditions, the fields can act as dark energy components in our setup. The other notable thing is that if $N \gg 1$, the quartic couplings of the χ field become much larger than the ϕ field, whereas the initial condition for the χ field becomes smaller and, in fact, sub-Planckian compatible with the swampland conjecture. Due to these, the χ field can play the role of a cascade field in our setup, which starts to oscillate around its minimum after the Hubble parameter squared drops below its mass, $\partial_\chi^2 V(\chi)$, and its energy density becomes a substantial part of the background energy density. This will lead to a sudden drop of the comoving sound horizon before the decoupling, which enhances

the Hubble parameter respectively today if the angular θ_{MC} parameter is fixed by the CMB experiments.

A similar model could be constructed in the context of multi-giant matrix vacua (Ashoorioon et al. 2010, 2009; Ashoorioon & Sheikh-Jabbari 2011, 2014) that uses concentric multiple stacks of D3-branes. In that model, the matrix structure of the coordinates perpendicular to the stack of D3-branes, and the ansatz of the $SU(2)$ generator for three of the orthogonal directions perpendicular to the stacks of D3-branes is used. To exploit the model to describe the late time Universe, with the string coupling $g_s \sim 1$, one has to use a large number of D3-branes, $N \sim 10^{40}$, and then one has to worry about backreaction effects of the D3-branes on the background geometry. Alternatively, one can assume that g_s itself is extremely small, say $g_s \sim 10^{-100}$ and further suppression of the quartic couplings of the fields to the required value to explain the dark energy vacuum density, $\lambda_{\phi, \chi} \sim 10^{-120}$ is achieved via the multiplicity of the D3-branes. Recently in Ashoorioon & Rezazadeh (2020), some of us showed that using a scalar field non-minimally coupled to gravity, with a moderate value of non-minimal coupling, one can reduce the required number of D3-branes to achieve the required number of D3-branes to a reasonable number during inflation. We will explore this scenario further in future work. Here, we instead focus on two minimally coupled scalar fields where their couplings, λ , are already small.

3. THE TWO-FIELD SETUP

In this work, we focus on the two-field realization of the CDE model, which consists of two dynamical scalar fields with canonical kinetic terms. The first Friedmann equation for a flat FRW Universe in this setup takes the following form

$$H^2 = \frac{1}{3M_P^2} (\rho_m + \rho_r + \rho_\phi + \rho_\chi), \quad (8)$$

where $H = \dot{a}/a$ is the Hubble parameter and $M_P \equiv 1/\sqrt{8\pi G}$ is the reduced Planck mass. Furthermore, ρ_m and ρ_r denote the energy densities of matter and radiation, respectively. The energy densities of the scalar field ϕ and χ are respectively denoted by ρ_ϕ and ρ_χ . It should be noted that in our work, we assume that the neutrinos are massless, and therefore their contribution is included in the energy density of the radiation component. The more general treatment of this setup requires also the inclusion of the massive neutrinos, and this possibility may be taken into account in future extensions of our scenario. It should also be noted that no definitive value for the mass of neutrinos has been reported so far.

The energy densities of matter and radiation vary with scale factor as follows

$$\rho_m = \rho_{mi} \left(\frac{a_i}{a} \right)^3, \quad (9)$$

$$\rho_r = \rho_{ri} \left(\frac{a_i}{a} \right)^4, \quad (10)$$

where ρ_{mi} and ρ_{ri} are the energy densities of matter and radiation, respectively, at the initial scale factor a_i that we take it deep inside in the radiation dominated era. We normalize these quantities as follows

$$\tilde{\rho}_{mi} \equiv \frac{\rho_{mi}}{M_P^2 H_0^2}, \quad (11)$$

$$\tilde{\rho}_{ri} \equiv \frac{\rho_{ri}}{M_P^2 H_0^2}, \quad (12)$$

where H_0 is the Hubble parameter today. We express the scale factor of the Universe in terms of the number of e -folds as

$$a = a_i e^N, \quad (13)$$

and hence from Eqs. (9) and (10), we find

$$\rho_m = M_P^2 H_0^2 \tilde{\rho}_{mi} e^{-3N}, \quad (14)$$

$$\rho_r = M_P^2 H_0^2 \tilde{\rho}_{ri} e^{-4N}. \quad (15)$$

The energy densities of the two canonical scalar fields are given by

$$\rho_\phi = \frac{1}{2} \dot{\phi}^2 + V_\phi(\phi), \quad (16)$$

$$\rho_\chi = \frac{1}{2} \dot{\chi}^2 + V_\chi(\chi). \quad (17)$$

We take the potential of both the scalar fields in the following quartic forms

$$V_\phi(\phi) = \frac{1}{4} \lambda_\phi \phi^4, \quad (18)$$

$$V_\chi(\chi) = \frac{1}{4} \lambda_\chi \chi^4, \quad (19)$$

where λ_ϕ and λ_χ are respectively the self-interaction coupling constants for the ϕ and χ fields. Applying the continuity equations for the energy densities Eqs. (16) and (17), we obtain the equations of motion for ϕ and χ , respectively, as

$$\ddot{\phi} + 3H\dot{\phi} + \frac{dV_\phi(\phi)}{d\phi} = 0, \quad (20)$$

$$\ddot{\chi} + 3H\dot{\chi} + \frac{dV_\chi(\chi)}{d\chi} = 0. \quad (21)$$

Now, following [Rezazadeh et al. \(2020\)](#), we introduce the following normalized quantities

$$\begin{aligned} \tilde{H} &\equiv \frac{H}{H_0}, & \tilde{\phi} &\equiv \frac{\phi}{M_P}, & \tilde{\chi} &\equiv \frac{\chi}{M_P}, \\ \tilde{\lambda}_\phi &\equiv \frac{M_P^2}{H_0^2} \lambda_\phi, & \tilde{\lambda}_\chi &\equiv \frac{M_P^2}{H_0^2} \lambda_\chi. \end{aligned} \quad (22)$$

As a result, from Eq. (8), we get

$$\tilde{H}^2 = \frac{4(\tilde{\rho}_{mi} e^{-3N} + \tilde{\rho}_{ri} e^{-4N}) + \tilde{\lambda}_\phi \tilde{\phi}^4 + \tilde{\lambda}_\chi \tilde{\chi}^4}{2(6 - \tilde{\phi}'^2 - \tilde{\chi}'^2)}, \quad (23)$$

where the prime denotes the derivative with respect to the e -fold number N . If we take the derivative of both sides of the above equation with respect to N , we obtain

$$\begin{aligned} \tilde{H}' = -\frac{1}{\tilde{H}(6 - \tilde{\phi}'^2 - \tilde{\chi}'^2)} &\left[3\tilde{\rho}_{mi} e^{-3N} + \tilde{\rho}_{ri} 4e^{-4N} \right. \\ &\left. - \tilde{H}^2 (\tilde{\phi}' \tilde{\phi}'' + \tilde{\chi}' \tilde{\chi}'') - \tilde{\lambda}_\phi \tilde{\phi}^3 \tilde{\phi}' - \tilde{\lambda}_\chi \tilde{\chi}^3 \tilde{\chi}' \right]. \end{aligned} \quad (24)$$

Applying the normalized quantities (22) in (20) and (21), we also reach

$$\tilde{\phi}'' = -\frac{\tilde{H}(3\tilde{H} + \tilde{H}') \tilde{\phi}' + \tilde{\lambda}_\phi \tilde{\phi}^3}{\tilde{H}^2}, \quad (25)$$

$$\tilde{\chi}'' = -\frac{\tilde{H}(3\tilde{H} + \tilde{H}') \tilde{\chi}' + \tilde{\lambda}_\chi \tilde{\chi}^3}{\tilde{H}^2}. \quad (26)$$

Inserting these into Eq. (24), and then solving the resulting equation for \tilde{H}' , we arrive at

$$\tilde{H}' = -\frac{1}{6\tilde{H}e^{4N}} \left[3\tilde{H}^2 (\tilde{\phi}'^2 + \tilde{\chi}'^2) e^{4N} + 3\tilde{\rho}_{mi} e^N + 4\tilde{\rho}_{ri} \right]. \quad (27)$$

To eliminate \tilde{H}' in Eqs. (25) and (26), we use the above equation and hence we will have

$$\begin{aligned} \tilde{\phi}'' = -\frac{1}{6\tilde{H}^2} &\left[e^{-4N} \tilde{\phi}' \left(3e^{4N} \tilde{H}^2 (6 - \tilde{\chi}'^2 - \tilde{\phi}'^2) \right. \right. \\ &\left. \left. - 3\tilde{\rho}_{mi} e^N - 4\tilde{\rho}_{ri} \right) + 6\tilde{\lambda}_\phi \tilde{\phi}^3 \right], \end{aligned} \quad (28)$$

$$\begin{aligned} \tilde{\chi}'' = -\frac{1}{6\tilde{H}^2} &\left[e^{-4N} \tilde{\chi}' \left(3e^{4N} \tilde{H}^2 (6 - \tilde{\chi}'^2 - \tilde{\phi}'^2) \right. \right. \\ &\left. \left. - 3\tilde{\rho}_{mi} e^N - 4\tilde{\rho}_{ri} \right) + 6\tilde{\lambda}_\chi \tilde{\chi}^3 \right]. \end{aligned} \quad (29)$$

Eqs. (27), (28), and (29), are basic equations that we will solve in our work to find the background dynamics. To determine the initial conditions, we assume that the evolution of the two scalar fields starts from the slow-roll regime. Therefore, the first term in Eqs. (20) and (21) can be neglected before the other terms, and these equations simplify as follows

$$3H\dot{\phi} + \frac{dV_\phi(\phi)}{d\phi} \approx 0, \quad (30)$$

$$3H\dot{\chi} + \frac{dV_\chi(\chi)}{d\chi} \approx 0, \quad (31)$$

which in turn can be written in terms of e -folds number as

$$\tilde{\phi}' \approx -\frac{\tilde{\lambda}_\phi \tilde{\phi}^3}{3\tilde{H}^2}, \quad (32)$$

$$\tilde{\chi}' \approx -\frac{\tilde{\lambda}_\chi \tilde{\chi}^3}{3\tilde{H}^2}. \quad (33)$$

Besides, in the slow-roll regime, the kinetic terms of ϕ and χ are negligible in comparison with their potentials, and therefore the Friedmann equation, Eq. (8), can be approximated as

$$H^2 \approx \frac{1}{3M_P^2} [\rho_m + \rho_r + V_\phi(\phi) + V_\chi(\chi)]. \quad (34)$$

If we substitute ρ_m and ρ_r from Eqs. (9) and (10), respectively, into this equation, and then use Eqs. (14), (15), (18), (19), and (22), we reach

$$\tilde{H}^2 \approx \frac{1}{12} \left[4(\tilde{\rho}_{mi}e^{-3N} + \tilde{\rho}_{ri}e^{-4N}) + \tilde{\lambda}_\phi \tilde{\phi}^4 + \tilde{\lambda}_\chi \tilde{\chi}^4 \right]. \quad (35)$$

This equation now can be inserted into Eqs. (32) and (33) to give the initial values of derivative of the two scalar fields with respect to N as

$$\tilde{\phi}'_i \approx -\frac{4\tilde{\lambda}_\phi \tilde{\phi}_i^3}{4(\tilde{\rho}_{mi} + \tilde{\rho}_{ri}) + \tilde{\lambda}_\phi \tilde{\phi}_i^4 + \tilde{\lambda}_\chi \tilde{\chi}_i^4}, \quad (36)$$

$$\tilde{\chi}'_i \approx -\frac{4\tilde{\lambda}_\chi \tilde{\chi}_i^3}{4(\tilde{\rho}_{mi} + \tilde{\rho}_{ri}) + \tilde{\lambda}_\phi \tilde{\phi}_i^4 + \tilde{\lambda}_\chi \tilde{\chi}_i^4}. \quad (37)$$

In these equations, $\tilde{\phi}_i$ and $\tilde{\chi}_i$ refer to the initial values of the scalar fields at the e -fold number $N_i = 0$. Because H , ϕ , and χ are all numerically evolved in our representation of the dynamics, accurate initial conditions are needed for all these quantities to avoid exciting undesirable numerical transients. It should be noted that we cannot use Eq. (35) as the initial condition for \tilde{H} , because it leads to self-inconsistency of the differential equations. Instead, to prevent this problem, we apply the following relation which follows from Eq. (23),

$$\tilde{H}_i^2 = \frac{4(\tilde{\rho}_{mi} + \tilde{\rho}_{ri}) + \tilde{\lambda}_\phi \tilde{\phi}_i^4 + \tilde{\lambda}_\chi \tilde{\chi}_i^4}{2(6 - \tilde{\phi}_i'^2 - \tilde{\chi}_i'^2)}. \quad (38)$$

For $\tilde{\phi}'$ and $\tilde{\chi}'$ in this equation, we substitute their values from the slow-roll equations (36) and (37), respectively.

To integrate the background equations (27), (28), and (29), we used the 8th-order Runge-Kutta algorithm. Our modified version of CAMB, (which we use with CosmoMC to obtain constraints on the CDE model), is available online². In order to ensure that the Universe always remains flat in our code for each set of

input parameters, we use the parameter $\tilde{\lambda}_\phi$ as a derived parameter. To determine this parameter numerically, we note that the total density parameter at the present epoch is equal to the unity for a flat Universe,

$$\Omega_{m0} + \Omega_{r0} + \Omega_{\phi0} + \Omega_{\chi0} = 1, \quad (39)$$

where the subscript “0” refers to the present time. From this equation, we find

$$\tilde{\lambda}_\phi = \frac{12 - \tilde{\lambda}_\chi \tilde{\chi}_0^4 - 2\tilde{\phi}_0'^2 - 2\tilde{\chi}_0'^2 - 12\Omega_{m0} - 12\Omega_{r0}}{\tilde{\phi}_0^4}. \quad (40)$$

We use a shooting method in our numerical code that tests different values for $\tilde{\lambda}_\phi$ in the above equation for each set of free parameters. After several steps, the code finally finds a suitable value for this parameter that satisfies this equation with enough precision. As a result the parameter $\tilde{\lambda}_\phi$ is treated as a derived parameter in our numerical analysis. By requiring the ϕ field to provide the energy density required for a flat universe today, we target scenarios in which the data require χ to act as an EDE field and ϕ to be the present-day DE.

4. NUMERICAL ANALYSIS

Here, we obtain observational constraints to the CDE model at the level of background dynamics, using recent cosmological data. We use the publicly available CosmoMC computational package (Lewis & Bridle 2002). In this work, we used the July 2019 version of CosmoMC. This code uses a Markov Chain Monte Carlo (MCMC) simulation to explore the parameter space of the model, using the Metropolis-Hastings algorithm (Lewis & Bridle 2002).

Our parameter space consists of $\{\Omega_b h^2, \Omega_c h^2, \theta_{MC}, \tau, A_s, n_s, \tilde{\phi}_i, \tilde{\chi}_i, \tilde{\lambda}_\chi\}$, where Ω_b and Ω_c denote the present-day density parameters for baryon and cold dark matter, h is the dimensionless Hubble constant $h \equiv H_0/(100 \text{ kms}^{-1} \text{ Mpc}^{-1})$, θ_{MC} refers to the ratio of the comoving sound horizon at decoupling to the comoving angular diameter distance to the surface of last scattering, τ indicates the optical depth, A_s implies the amplitude of the primordial scalar power spectrum, and n_s is the scalar spectral index. To obtain well-behaved sampling as described in Ade et al. (2014) [with helpful formulae from (Hu & Sugiyama 1996)], the parameter θ_{MC} is varied in CosmoMC. Then a bisection root finding method is used to obtain the appropriate H_0 value within the Λ CDM model. Observables are properly computed using our modified version of CAMB.

The parameters $\tilde{\phi}_i$ and $\tilde{\chi}_i$ denote the value of the scalar fields at the scale factor a_i taken to be deep inside the radiation-dominated era. The coupling constant $\tilde{\lambda}_\chi$

² <https://github.com/krezazadeh/CAMB-CDE-two-field>

that is used for the coupling constant of the χ scalar field, is treated as a free parameter in our MCMC analysis, while the parameter $\tilde{\lambda}_\phi$ is a derived parameter, as explained earlier.

The CosmoMC package computes the likelihood of cosmological parameters by including observational data from various sources. We include the combination of CMB, SNe Ia, BAO, and Riess et al. (2019) data sets in our work, and so multiplying the separate likelihoods for these data sets, the total likelihood will be $\mathcal{L} \propto e^{-\chi_{\text{total}}^2/2}$, where $\chi_{\text{total}}^2 = \chi_{\text{CMB}}^2 + \chi_{\text{SN}}^2 + \chi_{\text{BAO}}^2 + \chi_{\text{Riess2019}}^2$ encodes the deviation between the observational and theoretical results. These data sets were chosen because they are included for use with the standard latest public release of the CosmoMC code. In future work, we will apply the Cobaya (Torrado & Lewis 2021) or MontePython (Brinckmann & Lesgourgues 2019) simulation codes to leverage more current data. Following Poulin et al. (2019); Smith et al. (2020a); Poulin et al. (2021); Murgia et al. (2021), we terminate our MCMC analysis when the Gelman-Rubin convergence criterion (Gelman & Rubin 1992) fulfills $R - 1 < 0.1$. For the statistical analysis of the MCMC chains generated by CosmoMC, we use the publicly available GetDist package (Lewis 2019), and a burn-in fraction of 0.3.

To establish priors for CDE (and Rock ‘n’ Roll) parameters in our MCMC as well as an initial guess for best-fit values we begin by finding rough initial guesses for $\tilde{\chi}_i$, $\log(\tilde{\phi}_i)$, and $\log(\tilde{\lambda}_\chi)$ that reproduce published Rock ‘n’ Roll *Planck* values for H_0 , the redshift of peak CDE energy-density fraction z_c , peak CDE energy density-fraction $f(z_c)$, and Ω_Λ when numerically integrated using the equations in Sec. 3. We then obtain an initial estimate of best-fit parameters for Λ CDM + CDE parameters using a simple random-walk simulation. We begin by choosing the standard (but relatively broad) flat priors for the usual cosmological parameters, centered around Planck 2018 best-fit values (Aghanim et al. 2020a), as well as a trial range for CDE parameters: $\Omega_b h^2 \in [0.021, 0.024]$, $\Omega_c h^2 \in [0.10, 0.15]$, $\theta_{\text{MC}} \in [1.0, 1.1]$, $\tau \in [0.02, 0.09]$, $n_s \in [0.94, 1.0]$, $\ln(10^{10} A_s) \in [2.9, 3.2]$, $\tilde{\chi}_i \in [0.01, 0.8]$, and $\tilde{\lambda}_\chi \in [14.5, 15.5]$. An initial guess is made for CDE parameters $\log \tilde{\phi}_i$, $\tilde{\chi}_i$, $\log \tilde{\lambda}_\chi$ as well as Λ CDM parameters, and used to compute the likelihood for the full data set (see below) computed within CosmoMC.

Afterward, random guesses are made for all 8 parameters but are kept only if they improve the likelihood of the model, with a maximum of 100 iterations. The results are insensitive to the values/ranges initially chosen for $\log \tilde{\phi}_i$ and $\log \tilde{\lambda}_\chi$, and indicate a preferred value for $\tilde{\chi}_i \simeq 0.4 - 0.5$. We then use the same flat priors on

Λ CDM parameters and final simulation values to initialize a proper likelihood minimization within CosmoMC, whose initial values are used for the subsequent MCMC. A similar procedure was used for the Rock ‘n’ Roll and single-field DE models considered. We verified that the posterior probability distributions for $\log \tilde{\phi}_i$ and $\log \tilde{\lambda}_\chi$ are nearly as flat as the priors, justifying their use without loss of generality. The initial field value $\tilde{\chi}_i$ is well constrained in our MCMC and is contained in the assumed prior. The priors used are summarized in Table 1.

We incorporate the Planck 2018 CMB data for temperature and polarization at small (TT,TE,EE) and large (lowl+lowE) angular scales (Aghanim et al. 2020a,b). We additionally take into account the CMB lensing potential power spectrum measured in the multipole range $40 \leq \ell \leq 400$ (Aghanim et al. 2020c). The acoustic peaks are affected by the physics of the decoupling epoch, and their locations are sensitive to physical processes occurring between the decoupling epoch and today.

Type Ia supernovae are standardizable candles that have approximately the same absolute magnitude, once corrections for the width of their light curve are applied. Therefore, they are a powerful tool that can be used to probe the expansion history of the Universe. In our MCMC analysis, we use the Pantheon SN sample (Scolnic et al. 2018), which consists of magnitude measurements for 1048 SNe Ia with redshifts $0.01 < z < 2.3$. In future work, we will use the more recent Pantheon + sample (Scolnic et al. 2022).

The baryonic acoustic oscillation standard ruler provides a measurement of the angular diameter distance as a function of the cosmological redshift. BAO data can be used to constrain dark energy models. The pressure waves arising from cosmological inhomogeneities in the primordial baryon-photon plasma are imprinted on the CMB and the Large-Scale Structure (LSS) of the galaxy density field. The peak appearing in measurements of the large-scale galaxy correlation function is caused by BAOs. In our analysis, we use BAO measurements from the Baryon Oscillation Spectroscopic Survey (BOSS) (Alam et al. 2017) ($z \simeq 0.15$), the SDSS Main Galaxy Sample (Ross et al. 2015) ($z \simeq 0.15$), and the 6dFGS (Beutler et al. 2012) ($z \simeq 0.11$).

Finally, we include the Riess et al. (2019) determination of $H_0 = 74.03 \pm 1.42 \text{ km s}^{-1} \text{ Mpc}^{-1}$ (Riess et al. 2019) for the Hubble constant, based on 70 Cepheid observations in the LMC and observations of nearby Type-Ia supernovae. This determination is an independent constraint of the expansion rate of the local Universe in our computations.

Table 1. The priors used in our MCMC analysis. When parameters do not appear in a model, we indicate this with a hyphen. The format is [lower bound, upper bound], initial guess.

Parameter	Λ CDM	Single-field DE	Rock ‘n’ Roll	Two-field CDE
$\Omega_b h^2$	[0.021, 0.024], 0.023	[0.021, 0.024], 0.023	[0.021, 0.024], 0.023	[0.021, 0.024], 0.023
$\Omega_c h^2$	[0.11, 0.13], 0.12	[0.11, 0.13], 0.12	[0.11, 0.13], 0.12	[0.11, 0.13], 0.12
$100\theta_{MC}$	[1.02, 1.06], 1.04	[1.02, 1.06], 1.04	[1.02, 1.06], 1.04	[1.02, 1.06], 1.04
τ	[0.02, 0.09], 0.055	[0.02, 0.09], 0.055	[0.02, 0.09], 0.055	[0.02, 0.09], 0.055
$\ln(10^{10} A_s)$	[2.98, 3.12], 3.05	[2.98, 3.12], 3.05	[2.98, 3.12], 3.05	[2.98, 3.12], 3.05
n_s	[0.95, 0.99], 0.97	[0.95, 0.99], 0.97	[0.95, 0.99], 0.97	[0.95, 0.99], 0.97
$\log_{10}(\tilde{\phi}_i)$	-	[0.5, 2.0], 1.04	-	[0.5, 2.0], 1.04
$\tilde{\chi}_i$	-	-	[0.1, 1.0], 0.54	[0.10, 1.0], 0.54
$\log_{10}(\tilde{\lambda}_\chi)$	-	-	[13.0, 15.5], 14.6	[13.0, 15.5], 14.6

5. RESULTS

The resulting best-fit values and 68% confidence limit (CL) constraints for the parameters of the investigated models are shown in Table 2. In the table, we see that the results for our single-field DE model are less than 0.5σ away from the Λ CDM, and the results of the two-field CDE model are much less than 0.5σ different from those of the Rock ‘n’ Roll scenario. We also see that both the Λ CDM and single-field DE models return the 68% CL constraint for the present-day Hubble parameter as $H_0 = 68.60 \pm 0.41 \text{ km s}^{-1}\text{Mpc}^{-1}$, which disagrees with the value $H_0 = 74.03 \pm 1.42 \text{ km s}^{-1}\text{Mpc}^{-1}$ measured by Riess et al. (2019) by more than 3σ (Riess et al. 2019). We also note that there is a degeneracy between the Rock ‘n’ Roll/CDE parameter $\tilde{\chi}_i$ and the baryon density parameter $\Omega_b h^2$, but no degeneracy between $\Omega_b h^2$ and $\log(\tilde{\lambda}_\chi)$. The other standard Λ CDM parameters (e.g. n_s and τ , the optical depth to reionization) are not noticeably degenerate with Rock ‘n’ Roll/CDE model parameters.

The Rock ‘n’ Roll and two-field CDE models yield a best-fit value for H_0 of $H_0 = 70.43 \pm 0.99 \text{ km s}^{-1}\text{Mpc}^{-1}$ and $H_0 = 70.42 \pm 0.98 \text{ km s}^{-1}\text{Mpc}^{-1}$, respectively. These results are within less than 0.5σ from one another and also in much better agreement with the Riess et al. (2019) measurement than models with no EDE, reducing the H_0 tension to 2σ . The 2D contour plots of the two-field CDE and Rock ‘n’ Roll models which include the H_0 parameter are separated thoroughly from the contour plots of the Λ CDM and single-field DE models.

We see in Table 2 that the Rock ‘n’ Roll ($S_8 = 0.824 \pm 0.010$) and two-field CDE ($S_8 = 0.824 \pm 0.010$) scenarios yield higher values for the S_8 parameter by about 0.4σ compared with the Λ CDM ($S_8 = 0.820 \pm 0.010$) and single-field DE ($S_8 = 0.8204 \pm 0.0098$) frameworks, and hence their results show more deviations from the DES 3-year observations (Zürcher et al. 2022), which indicate that $S_8 = 0.797_{-0.013}^{+0.015}$. This is a common feature of EDE models (Poulin et al. 2019; Smith et al. 2020a; Karwal et al. 2022; Poulin et al. 2021; Murgia et al. 2021), although it is not statistically significant.

From Table 3, we see that the two-field CDE model yields a lower value for χ_{total}^2 than the Λ CDM or single-field DE models, but is a worse fit than the Rock ‘n’ Roll model ($\Delta\chi_{\text{total}}^2 = 0.35$). The table indicates that χ_{total}^2 in the two-field CDE model gets reduced relative to Λ CDM models and single-field DE by 4.36 and 4.5 respectively, but its value has increased by 0.35 compared to the Rock ‘n’ Roll setup. Although the χ_{total}^2 value in the Rock ‘n’ Roll scenario is less than the two-field CDE model ($\Delta\chi_{\text{total}}^2 = 0.35$), it is interesting to point out that the two-field CDE model is a better fit to the BAO data in comparison with the Rock ‘n’ Roll model ($\Delta\chi_{\text{BAO}}^2 = -2.46$) which implies that BAO data favor late-time evolution in the DE component.

Results for 1D likelihoods and 2D contour plots in the 68% and 95% CL regions are shown in Fig. 1. The graph indicates that the results of the single-field DE model are less than 0.5σ of those of the Λ CDM model, and also that the results of the two-field CDE model are within a 0.5σ interval of the Rock ‘n’ Roll results.

The value of τ , the optical depth parameter, decreases in the two-field CDE model, compared to the Λ CDM and single field DE scenario. In the Rock ‘n’ Roll model, the value of this parameter gets reduced relative to the two field CDE model by 1σ . Compared with Agrawal et al. (2019), our best-fit RnR values for A_s and n_s are further enhanced compared with Λ CDM.

These differences are likely due to the neglect of perturbations, and may be responsible for the fact that our best-fit RnR $\Delta\chi^2$ is -4.4 , rather than the -7.8 reported in Agrawal et al. (2019). An important factor in this change is worse agreement between our data and the SHOES data set, when marginalized over model parameters, which have been pushed into different regions of the posterior volume due to details of perturbations. Since the statistically preferred parameter region for ϕ is such that the field has not yet started coherently oscillating, the perturbations in ϕ should be relatively small and ϕ is approximately unclustered. We thus anticipate that the relative difference in $\Delta\chi^2$ between RnR and CDE is stable to the inclusion of perturbations. In any case,

Table 2. The best-fit values and 68% CL constraints for the parameters of the investigated models.

Parameter	Λ CDM		Single-field DE		Rock ‘n’ Roll		Two-field CDE	
	best fit	68% limits	best fit	68% limits	best fit	68% limits	best fit	68% limits
$\Omega_b h^2$	0.02260	0.02251 ± 0.00013	0.02253	0.02251 ± 0.00013	0.02298	0.02281 ± 0.00017	0.02285	0.02275 ± 0.00018
$\Omega_c h^2$	0.11827	0.11849 ± 0.00090	0.11869	0.11851 ± 0.00087	0.12173	0.1216 ± 0.0017	0.12049	0.1214 ± 0.0017
$100\theta_{MC}$	1.04116	1.04116 ± 0.00029	1.04108	1.04113 ± 0.00029	1.03963	1.03958 ± 0.00073	1.0402	1.03978 ± 0.00074
τ	0.0596	0.0568 ± 0.0071	0.0572	$0.0566^{+0.0064}_{-0.0072}$	0.0550	0.0540 ± 0.0074	0.0570	0.0540 ± 0.0074
$\ln(10^{10} A_s)$	3.048	3.046 ± 0.014	3.044	$3.046^{+0.013}_{-0.014}$	3.050	3.047 ± 0.014	3.053	3.047 ± 0.014
n_s	0.9686	0.9690 ± 0.0037	0.9698	0.9688 ± 0.0036	0.9710	0.9697 ± 0.0036	0.9709	0.9691 ± 0.0037
$\log(\tilde{\phi}_i)$	–	–	1.82	$2.56^{+1.3}_{-0.57}$	–	–	1.43	2.40 ± 0.92
$\tilde{\chi}_i$	–	–	–	–	0.517	$0.467^{+0.13}_{-0.075}$	0.392	$0.428^{+0.14}_{-0.082}$
$\log(\tilde{\lambda}_\chi)$	–	–	–	–	14.507	–	15.428	–
H_0	68.76	68.60 ± 0.41	68.57	68.60 ± 0.41	71.21	70.43 ± 0.99	70.23	70.42 ± 0.98
Ω_m	0.2980	0.7003 ± 0.0052	0.3004	0.2997 ± 0.0051	0.2854	0.2913 ± 0.0065	0.2906	0.2908 ± 0.0065
Ω_{DE}	0.7020	0.2997 ± 0.0052	0.6996	0.7003 ± 0.0051	0.7146	0.7087 ± 0.0065	0.7094	0.7092 ± 0.0065
σ_8	0.8201	0.8208 ± 0.0060	0.8210	0.8208 ± 0.0058	0.8394	0.837 ± 0.010	0.8351	0.837 ± 0.010
S_8	0.8173	0.820 ± 0.010	0.8216	0.8204 ± 0.0098	0.8188	0.824 ± 0.010	0.8220	0.824 ± 0.010
Age/Gyr	13.730	13.741 ± 0.019	13.724	13.739 ± 0.020	13.382	13.46 ± 0.12	13.532	13.49 ± 0.12
$\log(\tilde{\lambda}_\phi)$	–	–	–6.34	$-9.3^{+4.1}_{-4.8}$	–	–	–4.80	-8.7 ± 3.7
z_c	–	–	–	–	15700	16790^{+3000}_{-4000}	23500	15990 ± 4000
$f(z_c)$	–	–	–	–	0.078	0.052 ± 0.021	0.047	0.044 ± 0.022

Table 3. The resulting values of χ^2 for each model and each data set. The χ^2 values corresponding to different CMB measurements including the Planck lensing power spectrum reconstruction (χ^2_{lensing}), baseline high- ℓ Planck power spectra ($30 \leq \ell \leq 2508$) ($\chi^2_{\text{high}\ell}$), low- ℓ Planck temperature ($2 \leq \ell \leq 29$) ($\chi^2_{\text{low}\ell}$), and low- ℓ HFI EE polarization ($2 \leq \ell \leq 29$) (χ^2_{simall}), are also presented in the table. The table also includes the values of χ^2_{tot} and $\Delta\chi^2 = \chi^2_{\text{Model}} - \chi^2_{\Lambda\text{CDM}}$.

Parameter	Λ CDM		Single-field DE		Rock ‘n’ Roll		Two-field CDE	
	best fit	68% limits	best fit	68% limits	best fit	68% limits	best fit	68% limits
χ^2_{lensing}	8.68	9.10 ± 0.55	9.10	9.08 ± 0.50	9.25	9.70 ± 0.90	9.15	9.68 ± 0.88
$\chi^2_{\text{high}\ell}$	2348.84	2359.6 ± 5.8	2352.99	2359.7 ± 6.0	2350.79	2360.7 ± 5.8	2350.2	2360.4 ± 5.8
$\chi^2_{\text{low}\ell}$	23.04	22.91 ± 0.76	22.03	22.93 ± 0.73	23.02	23.07 ± 0.78	22.94	23.20 ± 0.80
χ^2_{simall}	397.16	397.2 ± 1.9	395.74	397.2 ± 1.8	395.99	396.8 ± 1.5	396.40	396.8 ± 1.5
χ^2_{CMB}	2777.72	2788.9 ± 5.9	2777.19	2788.9 ± 6.0	2779.06	2790.2 ± 6.0	2778.69	2790.0 ± 6.0
χ^2_{SN}	1034.74	1034.792 ± 0.083	1034.74	1034.80 ± 0.12	1034.87	1034.87 ± 0.12	1034.85	1034.97 ± 0.29
χ^2_{BAO}	5.78	5.89 ± 0.81	5.44	5.86 ± 0.82	9.79	7.9 ± 2.3	7.33	7.8 ± 2.1
$\chi^2_{\text{Riess2019}}$	13.79	14.7 ± 2.2	14.80	14.7 ± 2.2	3.95	6.9 ± 3.6	7.15	6.9 ± 3.5
χ^2_{total}	3832.03	–	3832.17	–	3827.67	–	3828.02	–
$\Delta\chi^2$	0.0	–	0.14	–	–4.36	–	–4.01	–

our work thus provides a specific model realization of the two-fluid scenario also explored using a fluid parameterization in Moshafi et al. (2022).

Figure 1 additionally shows that the likelihood is quite insensitive to $\tilde{\phi}_i$ and $\tilde{\lambda}_\chi$, as evidenced by the flatness of the posterior contours in these parameters. These facts merit some explanation. For any ϕ_i bigger than a threshold, a larger value can be compensated with a smaller value of $\log \lambda_\phi$ where $\lambda_\phi \phi_i^4$ is of order the observed cosmological constant. Regarding χ , we can apply the approximate expression for f_{EDE} from Smith et al. (2020a) in the anharmonic limit for $n = 2$ (corresponding to a $\lambda_i \phi_i^4$ potential), to find that $f_{\text{EDE}} \sim \chi_i^2 / M_{\text{pl}}^2$. The coupling thus drops out and is roughly unconstrained, while χ_i is related to f_{EDE} leading to a meaningful constraint.

There is a preferred value for $\tilde{\chi}_i$ in the two-field CDE and Rock ‘n’ Roll models, implying a non-vanishing contribution of EDE to the cosmic energy density.

In Fig. 2, we used the best-fit values of the parameters listed in Table 2 to plot the evolution of the Hubble parameter against redshift, showing that the Hubble parameter of the single-field DE model is coincident with Λ CDM. Also, the results of the Rock ‘n’ Roll and two-field CDE models are $\sim 1\sigma$ away from each other. Nevertheless, at both the earlier and late times, the Hubble parameter of the Rock ‘n’ Roll scenario exceeds the value in the two-field CDE model, yielding a greater H_0 .

Smaller values of the Hubble parameter at lower redshifts give better compatibility of the two-field CDE model with BAO data, compared to Rock ‘n’ Roll ($\Delta\chi^2_{\text{BAO}} = -2.46$). Simultaneous agreement with PAN-THEON and BAO data causes the ϕ field to be overconstrained by the data, limiting the ability of the CDE

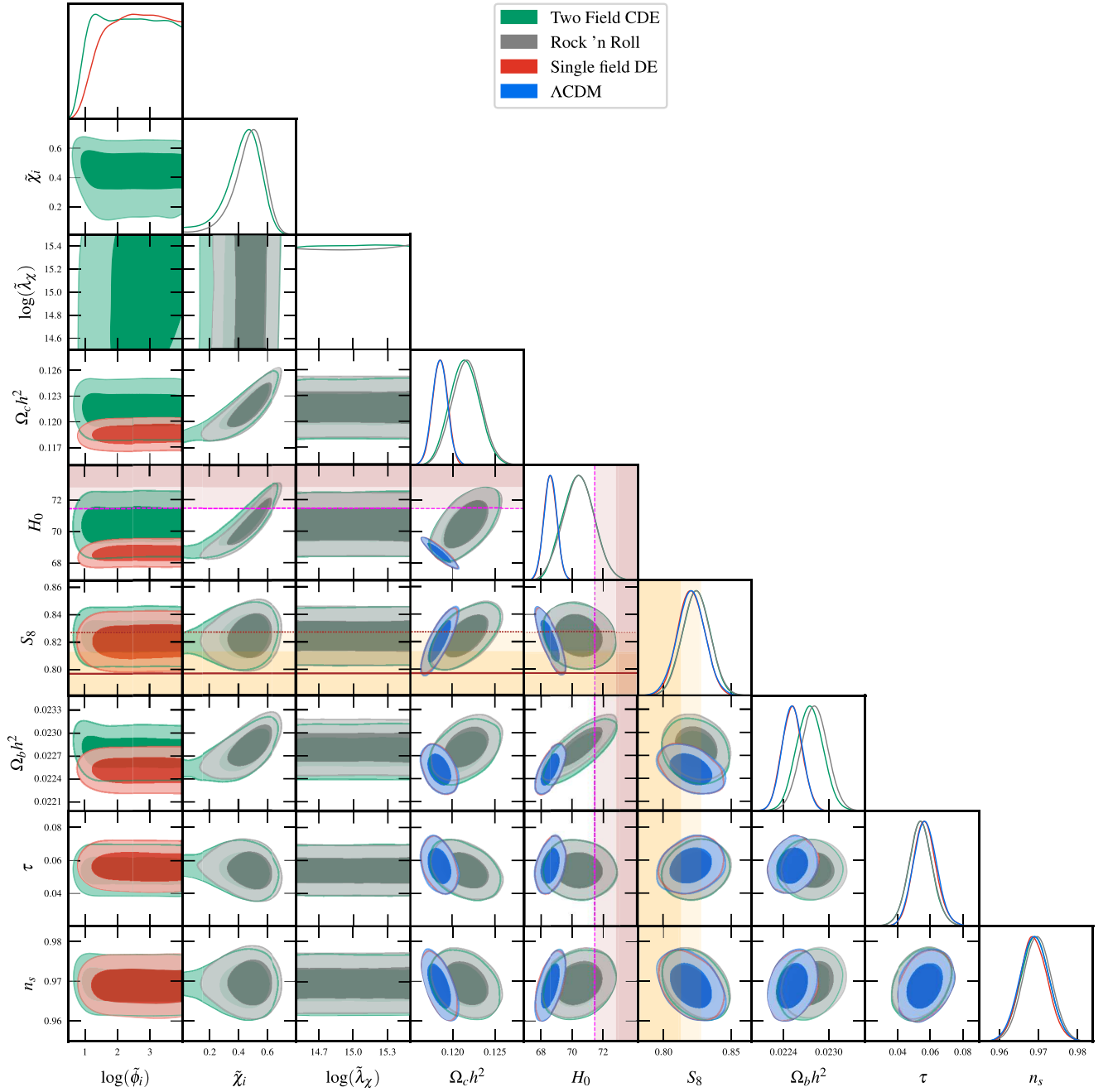


Figure 1. 1D likelihoods and 2D contours for the parameters in 68% and 95% CL marginalized joint regions for the Λ CDM model (blue), the single-field DE model (red), the rock ‘n’ roll model (gray), and the two-field CDE model (green). The logarithms for $\tilde{\phi}_i$ and $\tilde{\lambda}_\chi$ are base 10. The shaded regions in panels where one of the horizontal or vertical axes is H_0 from Riess et al. (2019). The shaded regions in panels where one of the horizontal or vertical axes is S_8 described in Zürcher et al. (2022). It should be noted that the 1σ regions of S_8 for the Λ CDM model contours in the figure overlap with the 1σ bands of DES estimation, so the selected data set is not in tension with the Λ CDM.

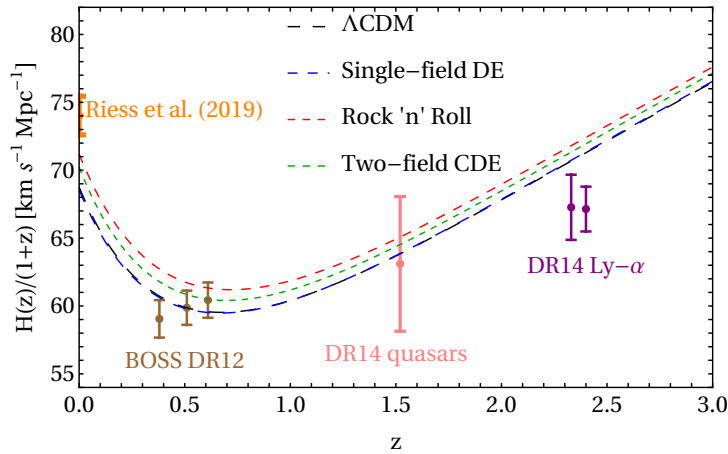


Figure 2. Evolution of the $H(z)/(1+z)$ as a function of cosmological redshift in the Λ CDM, single-field DE, Rock ‘n’ Roll, and two-field CDE models. Also, in the figure, the data points from (Riess et al. 2019), BOSS DR12 (Alam et al. 2017), DR14 quasars (Zarrouk et al. 2018), and DR14 Ly- α (Blomqvist et al. 2019) measurements have been specified for comparison. Note that only BOSS DR12 data were used to obtain the best-fit model parameters here.

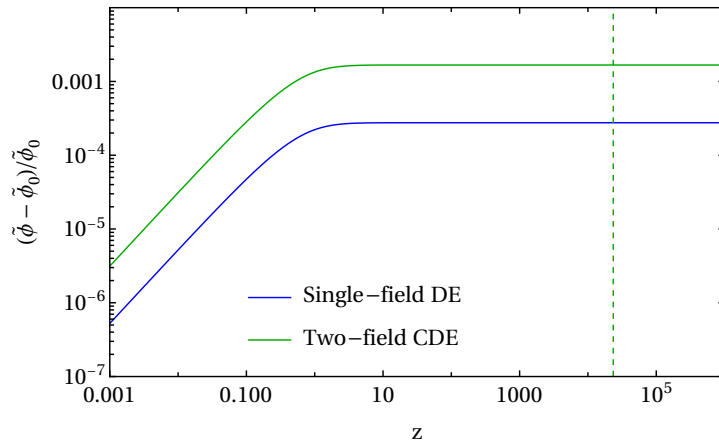


Figure 3. Evolution of the scalar field $\tilde{\phi}$ versus red-shift in the single-field DE and two-field CDE models, with a vertical dashed line indicating z_c in the two-field model.

model to better fit BAO data. It may be possible to go beyond this limitation by adding additional scalar fields. We have also developed a modified version of CAMB that has **three** dynamical fields (χ , ϕ , and a field ξ that rolls at an intermediate redshift). Preliminary exploration of some parameter combinations leads us to speculate that this scenario could provide a significantly better fit to lower- z BAO data (e.g. as in Fig. 2), but a proper MCMC analysis of this scenario using cosmological data awaits future work. As the 3 field-model is likely to begin coherent oscillation between recombination and the present-day dominance of dark energy, perturbations will become essential in obtaining the *relative* improvement of 3-field models over RnR and CDE. In pursuit of that scenario, we will compute the full perturbative dynamics of the 3-field scenario, taking advan-

tage of the more robust CLASS and Cobaya codes to ensure that this task is completed in a computationally efficient manner.

In Fig. 3, we show the evolution of the normalized scalar field $\tilde{\phi}$ in the single-field DE and two-field CDE models as a function of the scale factor. The accompanying scalar-field energy density $\tilde{\rho}_\phi$ is shown in Fig. 4. Aside from a small interval at late times, the scalar field $\tilde{\phi}$ tends to remain constant. But, around the present epoch, it becomes dynamic. The fractional variation of $\tilde{\phi}$ in the (best-fitting) single-field scenario is substantially greater than in the (best-fitting) two-field CDE scenario - this is because simultaneously allowing late and early-time dark energy allows the model to fit both the late-time acceleration of the Universe and provide the required early-time reduction in the sound horizon

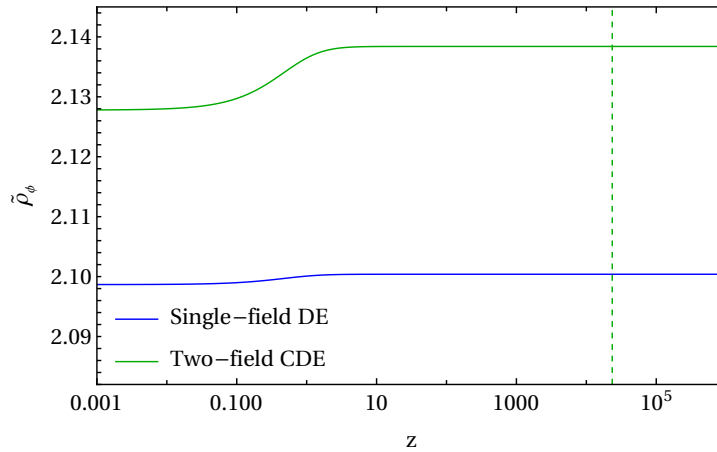


Figure 4. Evolution of the normalized scalar field energy density $\tilde{\rho}_\phi$ as a function of red-shift in the single-field DE and two-field CDE model, with a vertical dashed line indicating z_c in the two-field model.

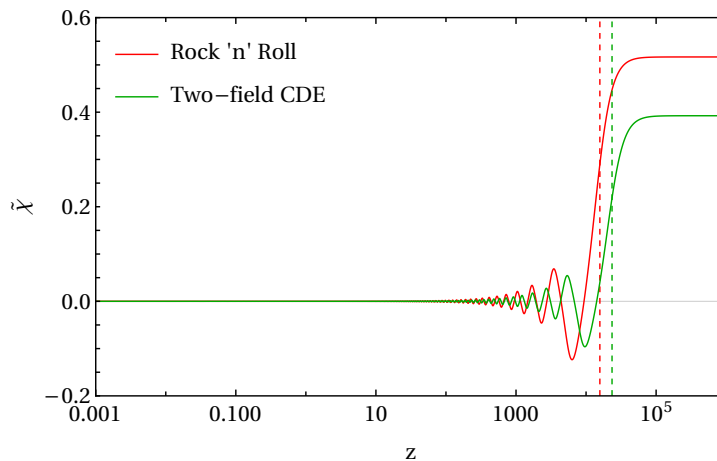


Figure 5. Evolution of the scalar field $\tilde{\chi}$ versus red-shift in the Rock ‘n’ Roll and two-field CDE models, with vertical dashed lines indicating z_c in both models.

needed to resolve the Hubble tension. In some sense, demanding less of the ϕ field allows its late-time behavior to more closely resemble Λ CDM.

In Fig. 5, the evolution of the scalar field $\tilde{\chi}$ as a function of scale factor is plotted for the Rock ‘n’ Roll and two-field CDE setups. Here we have used the best-fit values given in Table 2. The figure shows that the scalar field $\tilde{\chi}$ is almost constant at earlier times in these models, and after some time, it begins to oscillate around the potential minimum at $\tilde{\chi} = 0$. The initial value of $\tilde{\chi}$ is smaller in the two-field CDE model compared to the Rock ‘n’ Roll model, and consequently, its oscillations occur in this model earlier than in the Rock ‘n’ Roll model. At late times, the amplitude of the $\tilde{\chi}$ oscillations becomes very small, and accordingly, its contribution to the matter-energy content of the Universe becomes negligible.

In Fig. 6, we show the fraction of the EDE energy density relative to the total energy density, that is, $f_{\text{EDE}} \equiv \rho_\chi / \rho_{\text{total}}$. We see that f_{EDE} is negligible at the initial times, but after a while, it grows sharply and reaches a peak at the critical redshift z_c , and then it drops again and becomes very small at the late-times. For the Rock ‘n’ Roll model, the peak appears at the critical redshift $z_c = 1.57 \times 10^4$ with the maximum value $f_{\text{EDE}} = 0.078$. The peak of the two-field CDE model appears at $z_c = 2.35 \times 10^4$ with the maximum amplitude $f_{\text{EDE}} = 0.047$. The earlier peak energy of the two-field CDE model means that this variant of EDE has less of an impact on the sound horizon at recombination [Knox & Millea \(2020\)](#), and in turn explains the result of our MCMC analysis, which shows that the two-field model is $\sim 1\sigma$ worse in relieving the Hubble tension than the Rock ‘n’ Roll model.

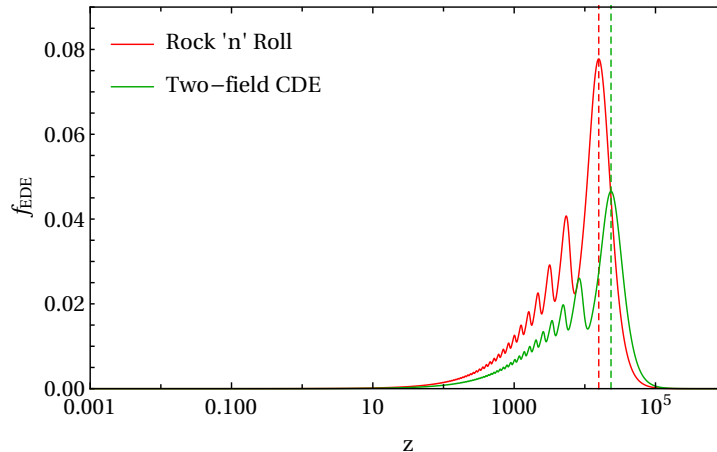


Figure 6. Evolution of the f_{EDE} as a function of cosmological redshift in the Rock ‘n’ Roll and two-field CDE models, with vertical dashed lines indicating z_c in both models.

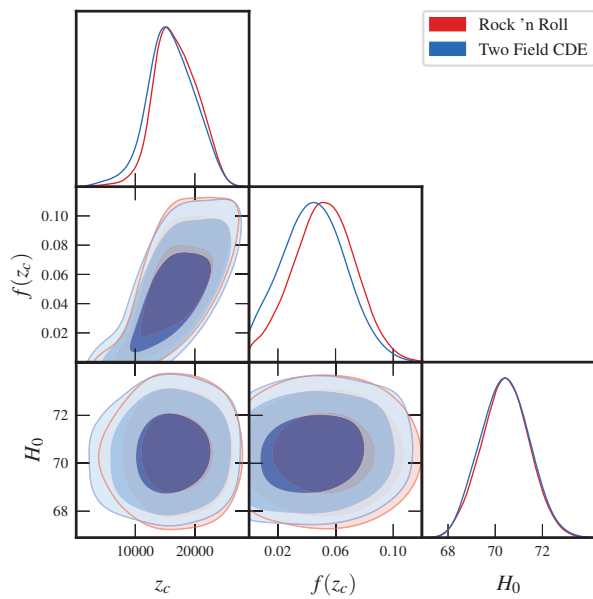


Figure 7. 68% and 95% CL marginalized 1D likelihoods and 2D contours of z_c , $f(z_c)$, and H_0 for the Rock ‘n’ Roll model (red), and the two-field CDE model (blue).

In prior work on EDE models, the parameters z_c and f_{EDE} [rather than model-specific parameters such as $\log(\tilde{\phi}_i)$, $\tilde{\chi}_i$, or $\log(\tilde{\lambda}_\chi)$] are sometimes varied in the MCMC. We output these parameters as derived values from CosmoMC (with an appropriate modification to CAMB), and show the resulting posteriors in Fig. 7 and Table 2. We see that there is a strong degeneracy between $f(z_c)$ and z_c in both EDE models considered. We verified that the data yield a significantly smaller allowed region than the effective prior for these derived

parameters. The difference between the best fit values z_c [or $f(z_c)$] obtained from likelihood and posterior in Fig. 6 results from the highly non-Gaussian posterior and range of $f(z_c)$ (or z_c) values which must be marginalized over.

Figure 8 shows the evolution of the equation of state parameter of dark energy, $w_{\text{DE}} \equiv p_{\text{DE}}/\rho_{\text{DE}} = (p_\phi + p_\chi)/(\rho_\phi + \rho_\chi)$, in terms of cosmological redshift. At high redshifts, w_{DE} begins at -1 , and subsequently oscillates around zero, with w_{DE} varying between -1 and 1 . Eventually, it converges to -1 and remains very close to this value until the present time. The oscillations of w_{DE} start sooner in the two-field CDE model than in the Rock ‘n’ Roll scenario, although the oscillations last longer for Rock ‘n’ Roll.

We present the residuals of CMB power spectra in Fig. 9. In the figure, we have also shown Planck 2018 data points (Aghanim et al. 2020a,b,c) for comparison. We see in the figure that the results of the single-field DE are indistinguishable from ΛCDM results, while the Rock ‘n’ Roll and two-field CDE models show deviations from ΛCDM , exceeding cosmic variance in some cases. To roughly estimate the improvement in constraining power of future CMB experiments, we compute the statistic (Grin & Hirata 2010)

$$\mathcal{Z} \equiv \sqrt{\sum_{\ell} \frac{\Delta C_{\ell}^2}{\sigma_{\ell}^2}}, \quad (41)$$

where the sum over the binned spectrum is evaluated using the deviation ΔC_{ℓ} of the model of interest, with binned cosmic variance errors used for σ_{ℓ} . We separately compute this sum for temperature and EE polarization. A full forecast requires a proper analysis of T and E covariances, or better yet, a full Fisher matrix analysis that properly accounts for parameter degeneracies in-

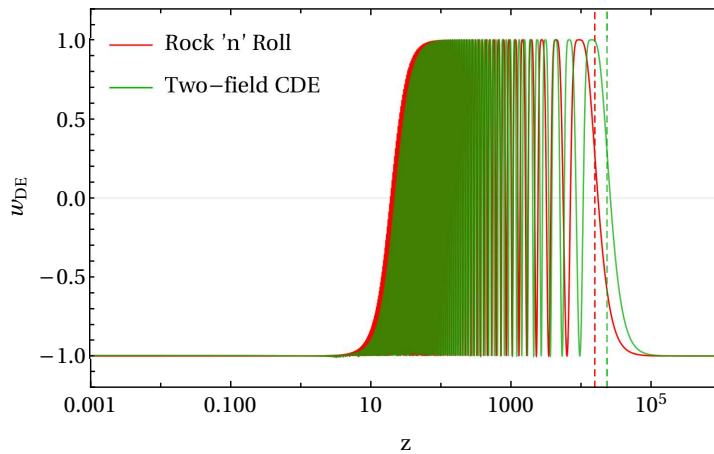


Figure 8. Evolution of the w_{DE} as a function of cosmological redshift in the Rock ‘n’ Roll and two-field CDE models.

cluding nuisance parameters). Nonetheless, this rough estimate can give us some sense of whether or not the CMB alone can detect deviations between the models we consider, with future data. Roughly speaking, \mathcal{Z} is the number of sigmas at which two scenarios can be distinguished.

Using temperature, we find that future data could distinguish between the single and two-field scenarios with $\sim 3\sigma$ significance, which improves to a $\sim 20\sigma$ potential detection in the limit that TE covariances vanish. Of course, this is not the case, and so a full Fisher matrix forecast is likely to show an answer closer to $\sim 7\sigma$ (ie, the geometric mean of the two extreme cases).

6. CONCLUSIONS

We studied the cascading dark energy model, in which many scalar fields contribute to the dark energy component of the Universe. In this setup, a large number of canonical scalar fields with sub-Planckian field excursions and steep potentials cooperate to provide a super-Planckian excursion and a relatively flat potential that can induce the late acceleration of the Universe as well as an early dark energy epoch. In the example we considered, the discordant initial conditions between fields cause some to cascade, drop out of the ensemble, and start oscillating around their minima. We restricted our attention to a single cascade involving an interplay reducing to an effective theory of two fields, ϕ , and χ . We choose the initial conditions such that ϕ plays the role of the late dark energy, while the χ field behaves as EDE, subsequently cascading and decaying quickly.

We used MCMC simulations to test CDE and related scenarios using CMB, BAO, PANTHEON observations of Type-Ia supernovae, and Riess et al. (2019) data. Our work shows that in the CDE model, χ^2_{total} gets reduced relative to Λ CDM and single-field DE models

by 4.01 and 4.15 respectively. In contrast, the CDE model’s χ^2_{total} is worse than the Rock ‘n’ Roll model with $\Delta\chi^2_{\text{total}} = 0.35$. The two-field CDE model yields a fit of $H_0 = 70.42 \pm 0.98 \text{ km s}^{-1}\text{Mpc}^{-1}$, substantially higher than Λ CDM ($H_0 = 68.60 \pm 0.41 \text{ km s}^{-1}\text{Mpc}^{-1}$) and single-field DE ($H_0 = 68.60 \pm 0.41 \text{ km s}^{-1}\text{Mpc}^{-1}$) values, while very close to the Rock ‘n’ Roll values ($H_0 = 70.43 \pm 0.99 \text{ km s}^{-1}\text{Mpc}^{-1}$).

The CDE and Rock ‘n’ Roll versions of the EDE scenario thus reduce the Hubble tension between supernovae ($H_0 = 74.03 \pm 1.42 \text{ km s}^{-1}\text{Mpc}^{-1}$) and other methods. Our analysis also shows that the two-field CDE model ($\chi^2_{\text{BAO}} = 7.33$) provides a modestly improved fit to BAO data compared with the Rock ‘n’ Roll model ($\chi^2_{\text{BAO}} = 9.79$). Of course this comes at the price of worse compatibility with the Riess H_0 data, which makes the overall χ^2 worse than the Rock ‘n’ Roll model.

There are a number of important avenues needed to expand and critically test our results. The analysis shown here did not follow the linear perturbations of either DE component - as noted, these do have a statistical impact on inferences about EDE properties, and in the future, we will generalize our analysis to include CDE clustering in the linear regime (Khorasani et al. in prep). We will also explore the possibility of rich resonant non-linear phenomenology, as discussed in Smith et al. (2020a). Another area for future work is the exploration of a broader range of potential energy functions, motivated by a variety of considerations.

Since the effective super-Planckian field samples the potential at relatively large values of the scalar field, the form of the potential at such values of the field can effectively be different from the part of the potential that only samples the sub-Planckian values of the field. For

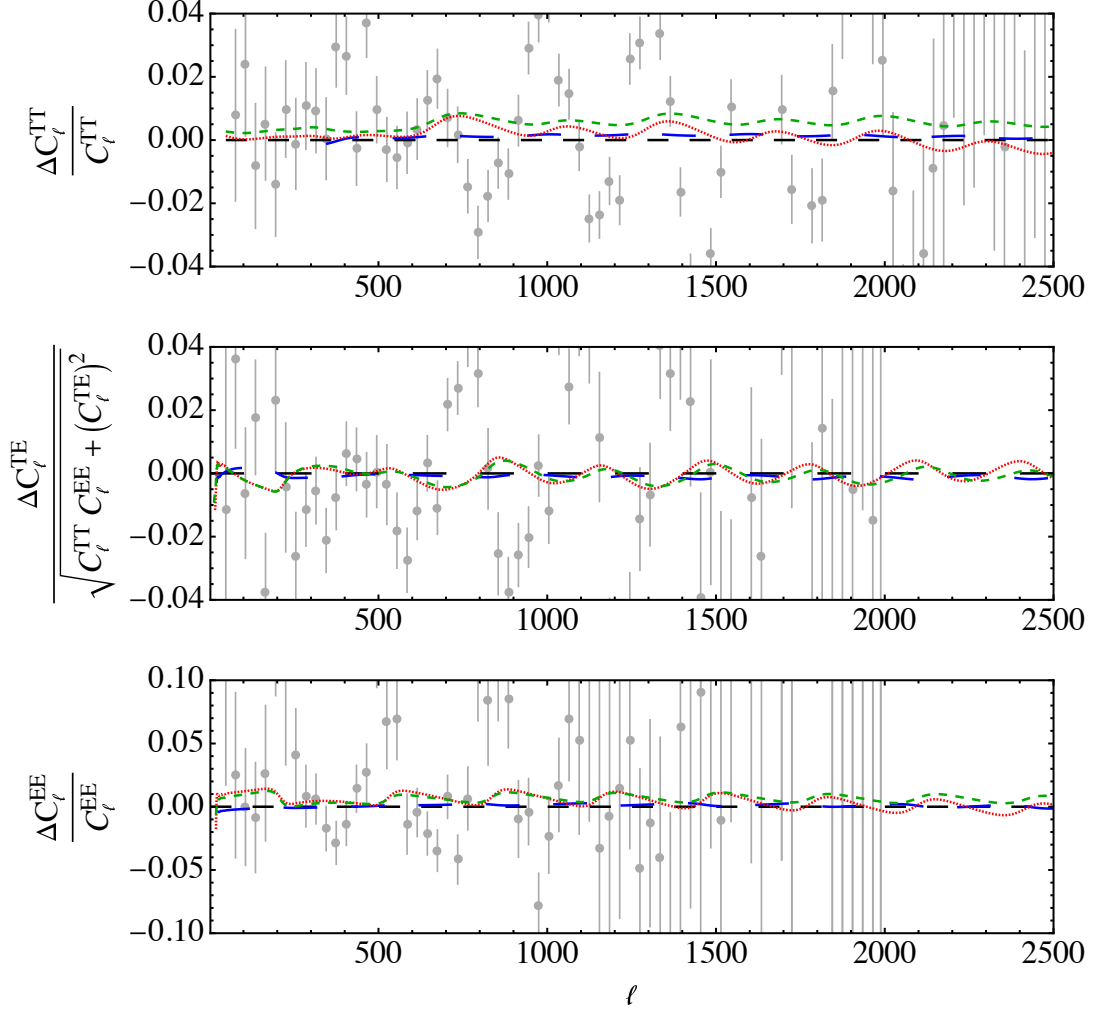


Figure 9. Residuals of the binned CMB power spectra relative to the reference Λ CDM model. The results of the Λ CDM (dashed black), single-field DE (long-dashed blue), Rock ‘n’ Roll (dotted red), and two-field CDE (short-dashed green) are compared with the binned Planck 2018 data points (gray) (Aghanim et al. 2020a,b,c). We compared models using the best-fit parameters for all cases.

example, the late field can effectively be on the parts of the potential that is just a cosmological constant. In this limit, the predictions and statistical significance of the model should be comparable approaches to the Rock ‘n’ Roll model. However, in principle, the late and early dark energy fields can have different potentials and this affects the predictions of the model. This is one interesting research avenue that is worth considering in the future.

Even with monomial potentials for both the late and early dark energy fields, one can assume non-renormalizable forms for the potentials. For example with a sixth-order monomial potential, ϕ^6 , we expect that the model can achieve larger values of H_0 , as shown in Poulin et al. (2019). The scalar fields also may have non-canonical kinetic terms. In particular, we can as-

sume the kinetic terms for the dark energy fields have a DBI form, which has well-based theoretical motivations (Ahn et al. 2009). In addition, although in this paper, we assumed that the late dark energy and the cascading fields are coupled to the Einstein gravity minimally, one can consider their non-minimal couplings with gravity too (Sakstein & Trodden 2020; Braglia et al. 2021; Karwal et al. 2022; McDonough et al. 2022). These possibilities are left for future investigation.

ACKNOWLEDGMENTS

D. G. acknowledges support in part by NASA ATP Grant No. 17-ATP17-0162, and the provost's office of Haverford College. We thank Tristan Smith for useful conversations. This project has received funding/support from the European Union's Horizon 2020 research and innovation programme under the Marie Skłodowska-Curie grant agreement No 860881-HIDDeN.

REFERENCES

- Abbott, T. M. C., et al. 2018a, *Mon. Not. Roy. Astron. Soc.*, 480, 3879, doi: [10.1093/mnras/sty1939](https://doi.org/10.1093/mnras/sty1939)
- . 2018b, *Phys. Rev. D*, 98, 043526, doi: [10.1103/PhysRevD.98.043526](https://doi.org/10.1103/PhysRevD.98.043526)
- . 2022, *Phys. Rev. D*, 105, 023520, doi: [10.1103/PhysRevD.105.023520](https://doi.org/10.1103/PhysRevD.105.023520)
- Addison, G. E., Watts, D. J., Bennett, C. L., et al. 2018, *Astrophys. J.*, 853, 119, doi: [10.3847/1538-4357/aaa1ed](https://doi.org/10.3847/1538-4357/aaa1ed)
- Ade, P. A. R., et al. 2014, *Astron. Astrophys.*, 571, A16, doi: [10.1051/0004-6361/201321591](https://doi.org/10.1051/0004-6361/201321591)
- Aghanim, N., et al. 2020a, *Astron. Astrophys.*, 641, A6, doi: [10.1051/0004-6361/201833910](https://doi.org/10.1051/0004-6361/201833910)
- . 2020b, *Astron. Astrophys.*, 641, A5, doi: [10.1051/0004-6361/201936386](https://doi.org/10.1051/0004-6361/201936386)
- . 2020c, *Astron. Astrophys.*, 641, A8, doi: [10.1051/0004-6361/201833886](https://doi.org/10.1051/0004-6361/201833886)
- Agrawal, P., Cyr-Racine, F.-Y., Pinner, D., & Randall, L. 2019. <https://arxiv.org/abs/1904.01016>
- Ahn, C., Kim, C., & Linder, E. V. 2009, *Phys. Rev. D*, 80, 123016, doi: [10.1103/PhysRevD.80.123016](https://doi.org/10.1103/PhysRevD.80.123016)
- Alam, S., et al. 2017, *Mon. Not. Roy. Astron. Soc.*, 470, 2617, doi: [10.1093/mnras/stx721](https://doi.org/10.1093/mnras/stx721)
- Allali, I. J., Hertzberg, M. P., & Rompineve, F. 2021, *Phys. Rev. D*, 104, L081303, doi: [10.1103/PhysRevD.104.L081303](https://doi.org/10.1103/PhysRevD.104.L081303)
- Arvanitaki, A., Dimopoulos, S., Dubovsky, S., Kaloper, N., & March-Russell, J. 2010, *Phys. Rev. D*, 81, 123530, doi: [10.1103/PhysRevD.81.123530](https://doi.org/10.1103/PhysRevD.81.123530)
- Asgari, M., et al. 2021, *Astron. Astrophys.*, 645, A104, doi: [10.1051/0004-6361/202039070](https://doi.org/10.1051/0004-6361/202039070)
- Ashoorioon, A., Firouzjahi, H., & Sheikh-Jabbari, M. M. 2009, *JCAP*, 06, 018, doi: [10.1088/1475-7516/2009/06/018](https://doi.org/10.1088/1475-7516/2009/06/018)
- . 2010, *JCAP*, 05, 002, doi: [10.1088/1475-7516/2010/05/002](https://doi.org/10.1088/1475-7516/2010/05/002)
- Ashoorioon, A., & Rezaazadeh, K. 2020, *JHEP*, 07, 244, doi: [10.1007/JHEP07\(2020\)244](https://doi.org/10.1007/JHEP07(2020)244)
- Ashoorioon, A., & Sheikh-Jabbari, M. M. 2011, *JCAP*, 06, 014, doi: [10.1088/1475-7516/2011/06/014](https://doi.org/10.1088/1475-7516/2011/06/014)
- . 2014, *Phys. Lett. B*, 739, 391, doi: [10.1016/j.physletb.2014.11.018](https://doi.org/10.1016/j.physletb.2014.11.018)
- Ballardini, M., Finelli, F., Umiltà, C., & Paoletti, D. 2016, *JCAP*, 05, 067, doi: [10.1088/1475-7516/2016/05/067](https://doi.org/10.1088/1475-7516/2016/05/067)
- Barreira, A., Li, B., Baugh, C., & Pascoli, S. 2014, *JCAP*, 08, 059, doi: [10.1088/1475-7516/2014/08/059](https://doi.org/10.1088/1475-7516/2014/08/059)
- Belgacem, E., Dirian, Y., Foffa, S., & Maggiore, M. 2018, *JCAP*, 03, 002, doi: [10.1088/1475-7516/2018/03/002](https://doi.org/10.1088/1475-7516/2018/03/002)
- Bernal, J. L., Verde, L., Jimenez, R., et al. 2021, *Phys. Rev. D*, 103, 103533, doi: [10.1103/PhysRevD.103.103533](https://doi.org/10.1103/PhysRevD.103.103533)
- Bernal, J. L., Verde, L., & Riess, A. G. 2016, *JCAP*, 10, 019, doi: [10.1088/1475-7516/2016/10/019](https://doi.org/10.1088/1475-7516/2016/10/019)
- Beutler, F., Blake, C., Colless, M., et al. 2011, *Mon. Not. Roy. Astron. Soc.*, 416, 3017, doi: [10.1111/j.1365-2966.2011.19250.x](https://doi.org/10.1111/j.1365-2966.2011.19250.x)
- . 2012, *Mon. Not. Roy. Astron. Soc.*, 423, 3430, doi: [10.1111/j.1365-2966.2012.21136.x](https://doi.org/10.1111/j.1365-2966.2012.21136.x)
- Birrer, S., et al. 2019, *Mon. Not. Roy. Astron. Soc.*, 484, 4726, doi: [10.1093/mnras/stz200](https://doi.org/10.1093/mnras/stz200)
- Blomqvist, M., et al. 2019, *Astron. Astrophys.*, 629, A86, doi: [10.1051/0004-6361/201935641](https://doi.org/10.1051/0004-6361/201935641)
- Bonvin, V., et al. 2017, *Mon. Not. Roy. Astron. Soc.*, 465, 4914, doi: [10.1093/mnras/stw3006](https://doi.org/10.1093/mnras/stw3006)
- Braglia, M., Ballardini, M., Finelli, F., & Koyama, K. 2021, *Phys. Rev. D*, 103, 043528, doi: [10.1103/PhysRevD.103.043528](https://doi.org/10.1103/PhysRevD.103.043528)
- Brinckmann, T., & Lesgourgues, J. 2019, *Phys. Dark Univ.*, 24, 100260, doi: [10.1016/j.dark.2018.100260](https://doi.org/10.1016/j.dark.2018.100260)
- Chen, C.-B., & Soda, J. 2023, *JCAP*, 06, 049, doi: [10.1088/1475-7516/2023/06/049](https://doi.org/10.1088/1475-7516/2023/06/049)
- Davari, Z., Marra, V., & Malekjani, M. 2020, *Mon. Not. Roy. Astron. Soc.*, 491, 1920, doi: [10.1093/mnras/stz3096](https://doi.org/10.1093/mnras/stz3096)
- Di Valentino, E., Linder, E. V., & Melchiorri, A. 2018, *Phys. Rev. D*, 97, 043528, doi: [10.1103/PhysRevD.97.043528](https://doi.org/10.1103/PhysRevD.97.043528)

- Di Valentino, E., Melchiorri, A., Linder, E. V., & Silk, J. 2017a, *Phys. Rev. D*, 96, 023523, doi: [10.1103/PhysRevD.96.023523](https://doi.org/10.1103/PhysRevD.96.023523)
- Di Valentino, E., Melchiorri, A., & Mena, O. 2017b, *Phys. Rev. D*, 96, 043503, doi: [10.1103/PhysRevD.96.043503](https://doi.org/10.1103/PhysRevD.96.043503)
- Di Valentino, E., Melchiorri, A., & Silk, J. 2016, *Phys. Lett. B*, 761, 242, doi: [10.1016/j.physletb.2016.08.043](https://doi.org/10.1016/j.physletb.2016.08.043)
- Efstathiou, G. 2021, *Mon. Not. Roy. Astron. Soc.*, 505, 3866, doi: [10.1093/mnras/stab1588](https://doi.org/10.1093/mnras/stab1588)
- Emami, R., Grin, D., Pradler, J., Raccanelli, A., & Kamionkowski, M. 2016, *Phys. Rev. D*, 93, 123005, doi: [10.1103/PhysRevD.93.123005](https://doi.org/10.1103/PhysRevD.93.123005)
- Freese, K., & Winkler, M. W. 2021, *Phys. Rev. D*, 104, 083533, doi: [10.1103/PhysRevD.104.083533](https://doi.org/10.1103/PhysRevD.104.083533)
- Gelman, A., & Rubin, D. B. 1992, *Statist. Sci.*, 7, 457, doi: [10.1214/ss/1177011136](https://doi.org/10.1214/ss/1177011136)
- Grin, D., & Hirata, C. M. 2010, *Phys. Rev. D*, 81, 083005, doi: [10.1103/PhysRevD.81.083005](https://doi.org/10.1103/PhysRevD.81.083005)
- Hikage, C., et al. 2019, *Publ. Astron. Soc. Jap.*, 71, 43, doi: [10.1093/pasj/psz010](https://doi.org/10.1093/pasj/psz010)
- Hildebrandt, H., et al. 2020, *Astron. Astrophys.*, 633, A69, doi: [10.1051/0004-6361/201834878](https://doi.org/10.1051/0004-6361/201834878)
- Hill, J. C., McDonough, E., Toomey, M. W., & Alexander, S. 2020, *Phys. Rev. D*, 102, 043507, doi: [10.1103/PhysRevD.102.043507](https://doi.org/10.1103/PhysRevD.102.043507)
- Hlozek, R., Grin, D., Marsh, D. J. E., & Ferreira, P. G. 2015, *Phys. Rev. D*, 91, 103512, doi: [10.1103/PhysRevD.91.103512](https://doi.org/10.1103/PhysRevD.91.103512)
- Hu, W., & Sugiyama, N. 1996, *Astrophys. J.*, 471, 542, doi: [10.1086/177989](https://doi.org/10.1086/177989)
- Ivanov, M. M., McDonough, E., Hill, J. C., et al. 2020, *Phys. Rev. D*, 102, 103502, doi: [10.1103/PhysRevD.102.103502](https://doi.org/10.1103/PhysRevD.102.103502)
- Jimenez, R., Cimatti, A., Verde, L., Moresco, M., & Wandelt, B. 2019, *JCAP*, 03, 043, doi: [10.1088/1475-7516/2019/03/043](https://doi.org/10.1088/1475-7516/2019/03/043)
- Kamionkowski, M., Pradler, J., & Walker, D. G. E. 2014, *Phys. Rev. Lett.*, 113, 251302, doi: [10.1103/PhysRevLett.113.251302](https://doi.org/10.1103/PhysRevLett.113.251302)
- Karwal, T., & Kamionkowski, M. 2016, *Phys. Rev. D*, 94, 103523, doi: [10.1103/PhysRevD.94.103523](https://doi.org/10.1103/PhysRevD.94.103523)
- Karwal, T., Raveri, M., Jain, B., Khoury, J., & Trodden, M. 2022, *Phys. Rev. D*, 105, 063535, doi: [10.1103/PhysRevD.105.063535](https://doi.org/10.1103/PhysRevD.105.063535)
- Khorasani, M., Rezazadeh, K., Grin, D., & Ashoorioon, A. in prep, in prep.
- Knox, L., & Millea, M. 2020, *Phys. Rev. D*, 101, 043533, doi: [10.1103/PhysRevD.101.043533](https://doi.org/10.1103/PhysRevD.101.043533)
- Krishnan, C., Colgáin, E. O., Sheikh-Jabbari, M. M., & Yang, T. 2021, *Phys. Rev. D*, 103, 103509, doi: [10.1103/PhysRevD.103.103509](https://doi.org/10.1103/PhysRevD.103.103509)
- Kumar, S., & Nunes, R. C. 2016, *Phys. Rev. D*, 94, 123511, doi: [10.1103/PhysRevD.94.123511](https://doi.org/10.1103/PhysRevD.94.123511)
- Lewis, A. 2019. <https://arxiv.org/abs/1910.13970>
- Lewis, A., & Bridle, S. 2002, *Phys. Rev. D*, 66, 103511, doi: [10.1103/PhysRevD.66.103511](https://doi.org/10.1103/PhysRevD.66.103511)
- Liddle, A. R., Mazumdar, A., & Schunck, F. E. 1998, *Phys. Rev. D*, 58, 061301, doi: [10.1103/PhysRevD.58.061301](https://doi.org/10.1103/PhysRevD.58.061301)
- Lin, M.-X., Raveri, M., & Hu, W. 2019, *Phys. Rev. D*, 99, 043514, doi: [10.1103/PhysRevD.99.043514](https://doi.org/10.1103/PhysRevD.99.043514)
- Loureiro, A., et al. 2022, *Astron. Astrophys.*, 665, A56, doi: [10.1051/0004-6361/202142481](https://doi.org/10.1051/0004-6361/202142481)
- Marsh, D. J. E. 2016, *Phys. Rept.*, 643, 1, doi: [10.1016/j.physrep.2016.06.005](https://doi.org/10.1016/j.physrep.2016.06.005)
- McDonough, E., Lin, M.-X., Hill, J. C., Hu, W., & Zhou, S. 2022, *Phys. Rev. D*, 106, 043525, doi: [10.1103/PhysRevD.106.043525](https://doi.org/10.1103/PhysRevD.106.043525)
- Millon, M., et al. 2020, *Astron. Astrophys.*, 639, A101, doi: [10.1051/0004-6361/201937351](https://doi.org/10.1051/0004-6361/201937351)
- Moshafi, H., Firouzjahi, H., & Talebian, A. 2022, *Astrophys. J.*, 940, 121, doi: [10.3847/1538-4357/ac9c58](https://doi.org/10.3847/1538-4357/ac9c58)
- Murakami, Y. S., Riess, A. G., Stahl, B. E., et al. 2023, *JCAP*, 11, 046, doi: [10.1088/1475-7516/2023/11/046](https://doi.org/10.1088/1475-7516/2023/11/046)
- Murgia, R., Abellán, G. F., & Poulin, V. 2021, *Phys. Rev. D*, 103, 063502, doi: [10.1103/PhysRevD.103.063502](https://doi.org/10.1103/PhysRevD.103.063502)
- Niedermann, F., & Sloth, M. S. 2021, *Phys. Rev. D*, 103, L041303, doi: [10.1103/PhysRevD.103.L041303](https://doi.org/10.1103/PhysRevD.103.L041303)
- . 2022, *Phys. Rev. D*, 105, 063509, doi: [10.1103/PhysRevD.105.063509](https://doi.org/10.1103/PhysRevD.105.063509)
- Nunes, R. C. 2018, *JCAP*, 05, 052, doi: [10.1088/1475-7516/2018/05/052](https://doi.org/10.1088/1475-7516/2018/05/052)
- Obied, G., Ooguri, H., Spodyneiko, L., & Vafa, C. 2018. <https://arxiv.org/abs/1806.08362>
- Ooguri, H., & Vafa, C. 2007, *Nucl. Phys. B*, 766, 21, doi: [10.1016/j.nuclphysb.2006.10.033](https://doi.org/10.1016/j.nuclphysb.2006.10.033)
- Pandey, K. L., Karwal, T., & Das, S. 2020, *JCAP*, 07, 026, doi: [10.1088/1475-7516/2020/07/026](https://doi.org/10.1088/1475-7516/2020/07/026)
- Poulin, V., Boddy, K. K., Bird, S., & Kamionkowski, M. 2018a, *Phys. Rev. D*, 97, 123504, doi: [10.1103/PhysRevD.97.123504](https://doi.org/10.1103/PhysRevD.97.123504)
- Poulin, V., Smith, T. L., & Bartlett, A. 2021, *Phys. Rev. D*, 104, 123550, doi: [10.1103/PhysRevD.104.123550](https://doi.org/10.1103/PhysRevD.104.123550)
- Poulin, V., Smith, T. L., Grin, D., Karwal, T., & Kamionkowski, M. 2018b, *Phys. Rev. D*, 98, 083525, doi: [10.1103/PhysRevD.98.083525](https://doi.org/10.1103/PhysRevD.98.083525)
- Poulin, V., Smith, T. L., Karwal, T., & Kamionkowski, M. 2019, *Phys. Rev. Lett.*, 122, 221301, doi: [10.1103/PhysRevLett.122.221301](https://doi.org/10.1103/PhysRevLett.122.221301)

- Ramadan, O. F., Karwal, T., & Sakstein, J. 2024, *Phys. Rev. D*, 109, 063525, doi: [10.1103/PhysRevD.109.063525](https://doi.org/10.1103/PhysRevD.109.063525)
- Renk, J., Zumalacárregui, M., Montanari, F., & Barreira, A. 2017, *JCAP*, 10, 020, doi: [10.1088/1475-7516/2017/10/020](https://doi.org/10.1088/1475-7516/2017/10/020)
- Rezazadeh, K., Asadzadeh, S., Fahimi, K., Karami, K., & Mehrabi, A. 2020, *Annals Phys.*, 422, 168299, doi: [10.1016/j.aop.2020.168299](https://doi.org/10.1016/j.aop.2020.168299)
- Riess, A. G., Casertano, S., Yuan, W., Macri, L. M., & Scolnic, D. 2019, *Astrophys. J.*, 876, 85, doi: [10.3847/1538-4357/ab1422](https://doi.org/10.3847/1538-4357/ab1422)
- Riess, A. G., et al. 2016, *Astrophys. J.*, 826, 56, doi: [10.3847/0004-637X/826/1/56](https://doi.org/10.3847/0004-637X/826/1/56)
- . 2018, *Astrophys. J.*, 861, 126, doi: [10.3847/1538-4357/aac82e](https://doi.org/10.3847/1538-4357/aac82e)
- . 2022a, *Astrophys. J. Lett.*, 934, L7, doi: [10.3847/2041-8213/ac5c5b](https://doi.org/10.3847/2041-8213/ac5c5b)
- Riess, A. G., Breuval, L., Yuan, W., et al. 2022b, *Astrophys. J.*, 938, 36, doi: [10.3847/1538-4357/ac8f24](https://doi.org/10.3847/1538-4357/ac8f24)
- Ross, A. J., Samushia, L., Howlett, C., et al. 2015, *Mon. Not. Roy. Astron. Soc.*, 449, 835, doi: [10.1093/mnras/stv154](https://doi.org/10.1093/mnras/stv154)
- Sabla, V. I., & Caldwell, R. R. 2021, *Phys. Rev. D*, 103, 103506, doi: [10.1103/PhysRevD.103.103506](https://doi.org/10.1103/PhysRevD.103.103506)
- Sakstein, J., & Trodden, M. 2020, *Phys. Rev. Lett.*, 124, 161301, doi: [10.1103/PhysRevLett.124.161301](https://doi.org/10.1103/PhysRevLett.124.161301)
- Scolnic, D., et al. 2022, *Astrophys. J.*, 938, 113, doi: [10.3847/1538-4357/ac8b7a](https://doi.org/10.3847/1538-4357/ac8b7a)
- Scolnic, D. M., et al. 2018, *Astrophys. J.*, 859, 101, doi: [10.3847/1538-4357/aab9bb](https://doi.org/10.3847/1538-4357/aab9bb)
- Shajib, A. J., et al. 2023, *Astron. Astrophys.*, 673, A9, doi: [10.1051/0004-6361/202345878](https://doi.org/10.1051/0004-6361/202345878)
- Smith, T. L., Poulin, V., & Amin, M. A. 2020a, *Phys. Rev. D*, 101, 063523, doi: [10.1103/PhysRevD.101.063523](https://doi.org/10.1103/PhysRevD.101.063523)
- Smith, T. L., Poulin, V., Bernal, J. L., et al. 2020b, <https://arxiv.org/abs/2009.10740>
- Sola, J., Gomez-Valent, A., Perez, J. d. C., & Moreno-Pulido, C. 2020, *Class. Quant. Grav.*, 37, 245003, doi: [10.1088/1361-6382/abbc43](https://doi.org/10.1088/1361-6382/abbc43)
- Torrado, J., & Lewis, A. 2021, *JCAP*, 05, 057, doi: [10.1088/1475-7516/2021/05/057](https://doi.org/10.1088/1475-7516/2021/05/057)
- Umiltà, C., Ballardini, M., Finelli, F., & Paoletti, D. 2015, *JCAP*, 08, 017, doi: [10.1088/1475-7516/2015/08/017](https://doi.org/10.1088/1475-7516/2015/08/017)
- Vafa, C. 2005. <https://arxiv.org/abs/hep-th/0509212>
- Vagnozzi, S. 2020, *Phys. Rev. D*, 102, 023518, doi: [10.1103/PhysRevD.102.023518](https://doi.org/10.1103/PhysRevD.102.023518)
- Valcin, D., Bernal, J. L., Jimenez, R., Verde, L., & Wandelt, B. D. 2020, *JCAP*, 12, 002, doi: [10.1088/1475-7516/2020/12/002](https://doi.org/10.1088/1475-7516/2020/12/002)
- Valcin, D., Jimenez, R., Verde, L., Bernal, J. L., & Wandelt, B. D. 2021, *JCAP*, 08, 017, doi: [10.1088/1475-7516/2021/08/017](https://doi.org/10.1088/1475-7516/2021/08/017)
- Zarrouk, P., et al. 2018, *Mon. Not. Roy. Astron. Soc.*, 477, 1639, doi: [10.1093/mnras/sty506](https://doi.org/10.1093/mnras/sty506)
- Zhao, G.-B., et al. 2017, *Nature Astron.*, 1, 627, doi: [10.1038/s41550-017-0216-z](https://doi.org/10.1038/s41550-017-0216-z)
- Zürcher, D., Fluri, J., Sgier, R., et al. 2022, *Monthly Notices of the Royal Astronomical Society*, 511, 2075